Neuron
Article

Photochemical Restoration of Visual Responses in Blind Mice

Aleksandra Polosukhina,[1] Jeffrey Litt,[2,6] Ivan Tochitsky,[2,6] Joseph Nemargut,[3] Yivgeny Sychev,[3] Ivan De Kouchkovsky,[2] Tracy Huang,[1] Katharine Borges,[2] Dirk Trauner,[5] Russell N. Van Gelder,[3,4] and Richard H. Kramer[1,2,*]
[1]Vision Science Graduate Group
[2]Department of Molecular and Cell Biology
University of California, Berkeley, Berkeley, CA 94720, USA
[3]Department of Ophthalmology
[4]Department of Biological Structure
University of Washington, Seattle, WA 98195, USA
[5]Department of Chemistry and Biochemistry, University of Munich, D-81377 Munich, Germany
[6]These authors contributed equally to this work
*Correspondence: rhkramer@berkeley.edu
http://dx.doi.org/10.1016/j.neuron.2012.05.022

SUMMARY

Retinitis pigmentosa (RP) and age-related macular degeneration (AMD) are degenerative blinding diseases caused by the death of rods and cones, leaving the remainder of the visual system intact but largely unable to respond to light. Here, we show that AAQ, a synthetic small molecule photoswitch, can restore light sensitivity to the retina and behavioral responses in vivo in mouse models of RP, without exogenous gene delivery. Brief application of AAQ bestows prolonged light sensitivity on multiple types of retinal neurons, resulting in synaptically amplified responses and center-surround antagonism in arrays of retinal ganglion cells (RGCs). Intraocular injection of AAQ restores the pupillary light reflex and locomotory light avoidance behavior in mice lacking retinal photoreceptors, indicating reconstitution of light signaling to brain circuits. AAQ and related photoswitch molecules present a potential drug strategy for restoring retinal function in degenerative blinding diseases.

INTRODUCTION

Inherited degenerative diseases of the retina including retinitis pigmentosa (RP) affect 1 in 3,000 people worldwide. As differentiation of rods and cones ceases soon after birth in mammals, disorders resulting in photoreceptor degeneration lead to a permanent visual deficit. At present, there is no effective treatment for preventing this degenerative process and without some means of restoring photoreception, patients with advanced RP face the prospect of irreversible blindness.

Retinal ganglion cells (RGCs) are the sole output neurons of the retina. Hence, all of the visual information that reaches the brain is encoded by the spatial and temporal pattern of RGC action potentials. Several strategies have been advanced to enable light to alter RGC firing in the absence of rods and cones, with the goal of restoring visual function after the photoreceptors are lost (Jiménez et al., 1996; Marc et al., 2003; Punzo and Cepko, 2007; Strettoi and Pignatelli, 2000). First, biomedical engineers have developed surgically implanted retinal "chip" prosthetics (Chader et al., 2009; Gerding et al., 2007; Shire et al., 2009) that can be electronically controlled by an external camera to enable optical stimuli to trigger RGC firing. Retinal implants have restored simple shape discrimination to blind patients (Humayun et al., 2003; Yanai et al., 2007), indicating that artificial stimulation of RGCs in vivo can create a useful visual experience. Second, genes encoding optogenetic tools, including light-activated ion channels (Bi et al., 2006; Lagali et al., 2008; Tomita et al., 2010), transporters (Busskamp et al., 2010), or receptors (Caporale et al., 2011; Lin et al., 2008), can be introduced with viruses to bestow light-sensitivity on retinal neurons that survive after the natural photoreceptive cells have degenerated. Expression of optogenetic proteins in RGCs (Caporale et al., 2011; Tomita et al., 2010), bipolar cells (Lagali et al., 2008), and remnant cones (Busskamp et al., 2010) can reinstate light-elicited behavioral responses in mouse models of RP. Third, embryonic stem cells can be differentiated into photoreceptor progenitors in vitro (Lamba et al., 2006). Injecting these progenitors into blind animals results in integration of photoreceptors in the retina and restoration of some electrical activity in response to light (Lamba et al., 2009).

Each of these strategies has shown promise for restoring visual function, but they all require highly invasive and/or irreversible interventions that introduce hurdles to further development as a therapeutic approach. Implantation of retinal chips or stem cell-derived photoreceptors requires invasive surgery, while exogenous expression of optogenetic tools leads to permanent genetic alterations in retinal neurons. Retinal chip prosthetics rely on extracellular electrical stimulation of RGCs, which can be cytotoxic when excessive (Winter et al., 2007). Stem cell therapies carry potential for teratoma formation (Chaudhry et al., 2009). Viruses that deliver optogenetic tools can have off-target effects and may elicit inflammatory responses (Beltran et al., 2010). While the potential permanence

of optoelectronic, stem cell, or optogenetic interventions could be favorable in the absence of complications, any deleterious effects of these treatments could be very difficult or impossible to reverse.

Here, we report an alternative strategy for restoring visual function, based on a small molecule "photoswitch" that bestows light sensitivity onto neurons without requiring exogenous gene expression. The photoswitch is injected into the vitreous cavity of the eye, but unlike the other strategies, it does not require highly invasive surgical interventions and its actions are reversible. We used acrylamide-azobenzene-quaternary ammonium (AAQ), a K^+ channel photoswitch that enables optical control of neuronal excitability (Banghart et al., 2009; Fortin et al., 2008). AAQ was originally thought to conjugate to K^+ channels (Fortin et al., 2008), but recent work shows that the molecule interacts noncovalently with the cytoplasmic side of the channels, similar to the mechanism of action of local anesthetics (Banghart et al., 2009). The *trans* form of AAQ blocks K^+ channels and increases excitability, whereas photoisomerization to the *cis* form with short wavelength light (e.g., 380 nm) unblocks K^+ channels and decreases excitability. Relaxation from *cis* to *trans* occurs slowly in darkness but much more rapidly in longer-wavelength light (e.g., 500 nm), enabling rapid bi-directional photocontrol of neuronal firing with different wavelengths.

We show that AAQ confers robust light responses in RGCs in retinas from mutant mice that lack rods and cones. Moreover, after a single intraocular injection, AAQ restores light-driven behavior in blind mice in vivo. Because it is a rapid and reversible drug-like small molecule, AAQ represents a class of compounds that has potential for the restoration of visual function in humans with end-stage photoreceptor degenerative disease.

RESULTS

Imparting Light Sensitivity on rd1 Mouse Retina with AAQ

We tested whether AAQ can impart light sensitivity on retinas from 6-month-old *rd1* mice, a murine model of RP. The homozygous rd1 mouse (*rd1/rd1*) has a mutation in the gene encoding the β-subunit of cGMP phosphodiesterase-6, essential for rod phototransduction. Rods and cones in these mice degenerate nearly completely within 3 months after birth, leading to a loss of electrical and behavioral light responses (Sancho-Pelluz et al., 2008). We placed the rd1 mouse retina onto a multi-electrode array (MEA) that enables simultaneous extracellular recording from many RGCs (Meister et al., 1994). Before AAQ application, light generated no measurable change in RGC firing. However, after 30 min of treatment with AAQ, nearly all RGCs responded to light (Figure 1A). Photosensitization increased with AAQ concentration (Figure S1; Table S1 available online), but we used 300 μM for our standard ex vivo treatment. Light responses slowly diminished but were still robust for >5 hr after removing AAQ from the bathing medium (Figure S2a). Light responses could also be detected in three of four recordings from retinas removed from rd1 mice that had received in vivo intravitreal AAQ injections 12 hr previously (Figure S2b). The degree of photosensitivity varied, reflecting inaccurate injection in the small intravitreal volume of the mouse eye (2–3 μl).

Most RGCs exhibited an increase in firing rate in response to 380 nm light and a decrease in 500 nm light, opposite to AAQ-mediated light responses in neurons in culture (Fortin et al., 2008). To quantify the effects of light, we calculated a photoswitch index (PI), representing the normalized change in firing rate upon switching from darkness to 380 nm light. Positive or negative PI values reflect an increase or decrease, respectively, of firing. Before AAQ treatment, RGCs had almost no light response (median PI = 0.02); but after treatment, nearly all were activated by 380 nm light (median PI = 0.42) (Figure 1B). The rare light responses before AAQ treatment might result from melanopsin-containing intrinsically photosensitive RGCs (ipRGCs), which account for ~3% of the RGCs in the adult mouse retina (Hattar et al., 2002). Significant photosensitization was observed in each of 21 AAQ-treated retinas. On average, we observed an ~3-fold increase in RGC firing rate in response to 380 nm light, with individual retinas showing up to an 8-fold increase (Figure 1C).

AAQ Acts on RGCs, Bipolar, and Amacrine Cells in rd1 Retinas

We were surprised that 380 nm light stimulated RGC firing because this wavelength unblocks K^+ channels, which should reduce neuronal excitability. However, since RGCs receive inhibitory input from amacrine cells, RGC stimulation might be indirect, resulting from amacrine cell-dependent disinhibition. To test this hypothesis, we applied antagonists of receptors for GABA and glycine, the two inhibitory neurotransmitters released by amacrine cells. Photosensitization of RGCs by AAQ persisted after adding inhibitors of $GABA_A$, $GABA_C$, and glycine receptors (Figure 2A), but the polarity of photoswitching was reversed, with nearly all neurons inhibited rather than activated by 380 nm light (Figure 2B). These results indicate that photoregulation of amacrine cells is the dominant factor that governs the AAQ-mediated light response of RGCs.

After blocking amacrine cell synaptic transmission, the remaining light response could result from photoregulation of K^+ channels intrinsic to RGCs and/or photoregulation of excitatory inputs from bipolar cells. To explore the contribution of intrinsic K^+ channels, we obtained whole-cell patch clamp recordings from RGCs and pharmacologically blocked nearly all synaptic inputs (glutamatergic, GABAergic, and glycinergic). Depolarizing voltage steps activated outward K^+ currents that were smaller and decayed more rapidly in 500 nm light than in 380 nm light (Figure 2C). Comparison of current versus voltage (I-V) curves shows that the current was reduced by ~50% in 500 nm light (Figure 2D), similar to previous results (Fortin et al., 2008). However, MEA recordings indicate that photoregulation of RGC firing was nearly eliminated by blocking all excitatory and inhibitory synaptic inputs (Figure S3), suggesting that the light response is driven primarily by photoregulation of upstream neurons synapsing with RGCs.

To examine directly the contribution of retinal bipolar cells to the RGC light response, we blocked RGC K^+ channels with intracellular Cs^+ and added GABA and glycine receptor antagonists to block amacrine cell inputs. Flashes of 500 nm light triggered excitatory postsynaptic currents (EPSCs) in RGCs, and 380 nm light suppressed these events (Figures 2E and 2F). Blocking glutamate receptors eliminated these events, and bipolar cells

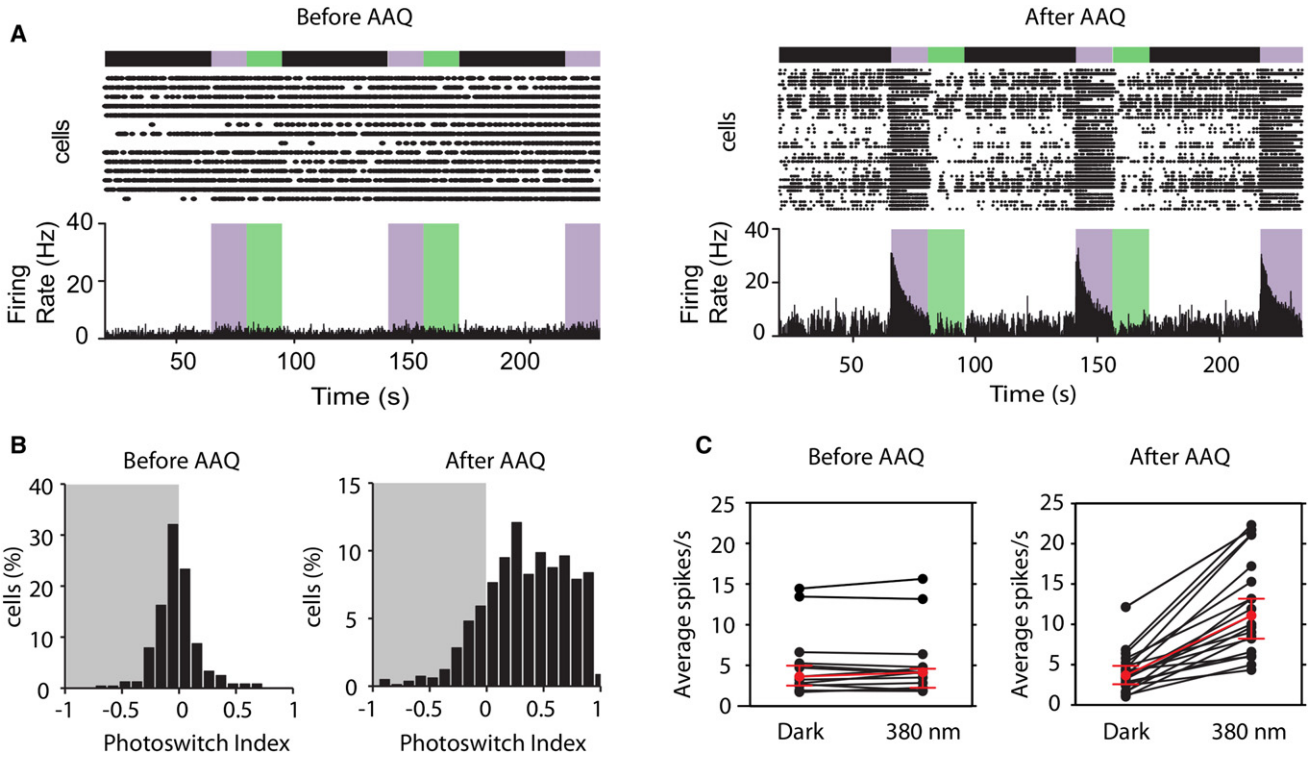

Figure 1. AAQ Imparts Light Sensitivity onto Blind Retinas from *rd1* Mice

(A) Multi-electrode recordings from a flat-mounted *rd1* mouse retina before and after treatment with AAQ (300 μM for 25 min, followed by washout). Top: Raster plot of spiking from RGCs. Bottom: Average RGC firing rate calculated in 100 ms time bins. Color bars represent illumination with 380 nm (violet) or 500 nm light (green), separated by periods of darkness (black).

(B) Analysis of photoswitching of the entire population of RGCs from all untreated retinas and all AAQ-treated retinas. Untreated retinas (n = 12) had PI values near 0, indicating no photoswitching, AAQ-treated retinas (n = 21) had PI values >0, indicating an increase in firing frequency after switching from darkness to 380 nm light.

(C) AAQ-mediated photosensitivity results from an increase in firing rate in 380 nm light. Average RGC firing rates in untreated retinas and AAQ-treated retinas in darkness and during the first 5 s in 380 nm light. Note that untreated retinas (n = 12) fail to respond to light, but AAQ-treated retinas have RGCs that increase firing rate with 380 nm light. Red symbols show median values and error bars represent 95% confidence intervals for untreated and treated retinas ($p < 0.0001$, Mann-Whitney test).

See also Figures S1 and S2.

provide the only known glutamatergic input to RGCs. Hence, we conclude that inputs from amacrine cells, bipolar cells, and to a lesser extent, the intrinsic K^+ conductances of RGCs, all combine to shape and amplify the AAQ-mediated RGC light response.

Spatial Localization and Center-Surround Antagonism of RGC Light Responses in AAQ-Treated Retina

Visual acuity is determined by the size of receptive fields of neurons in the visual system. In the healthy retina, the receptive field of an RGC is defined by the spatial extent of all of the photoreceptors that influence its activity. By definition, the receptive fields of RGCs in rd1 mice are eliminated after the photoreceptors have degenerated. However because AAQ makes presynaptic neurons light-sensitive, it is possible to measure the spatial extent of their light-driven influence on RGC firing. While this is not a conventional measurement of the RGC receptive field, it does indicate the spatial precision of the AAQ-mediated RGC light response.

We illuminated AAQ-treated retinas with small spots (60 μm diameter) of 380 nm light centered on one of the 60 electrodes in an MEA (Figure 3A). In the example shown in Figure 3A, upon switching from 500 to 380 nm light, the average RGC activity increased in the targeted electrode by ~81% but not in the surrounding electrodes. In each of a total of eight targeted spots from three different retinas, only neurons near the targeted electrode exhibited a significant increase in firing (median PI = 0.517; Figure 3B). Since RGCs are detected by only one electrode and they are spaced 200 μm apart, this puts an upper limit on the radius of the AAQ-mediated RGC collecting area of 100 μm.

Analysis of electrodes outside the illuminated spot showed that 380 nm light significant decreased RGC firing. Decreased firing was detected in electrodes centered at 300, 500, and 700 μm from the mid-point of the targeted electrode (Figure 3C; Table 1). Hence, RGCs in the center of an illuminated spot are stimulated, whereas those in a surrounding annulus (from 200 to 800 μm) are inhibited. Inhibition in the surrounding

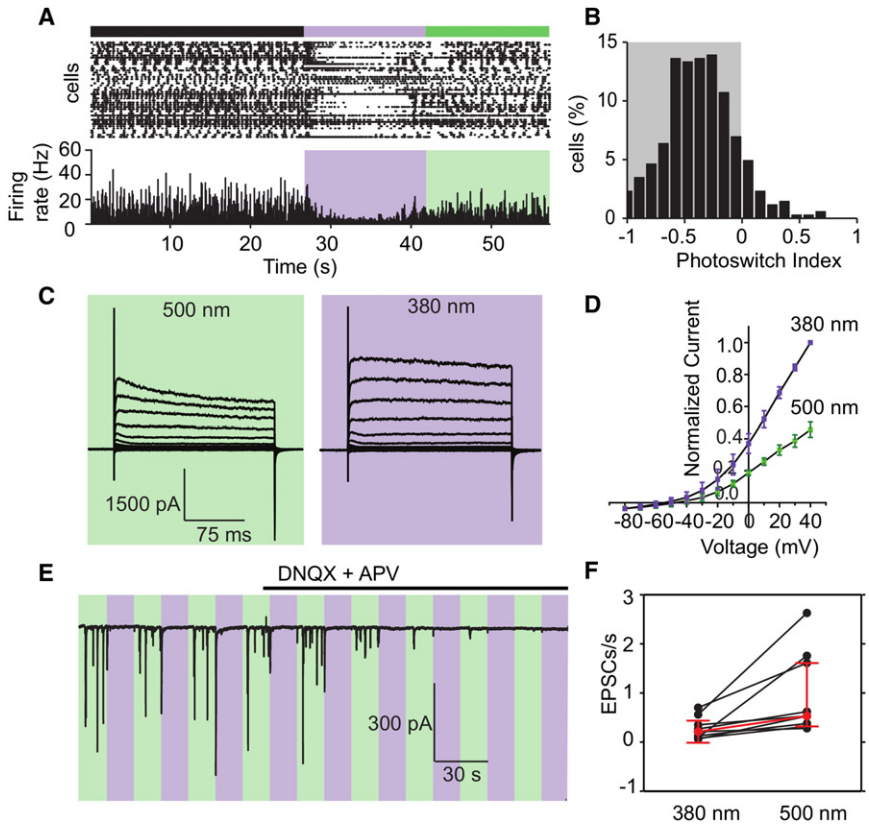

Figure 2. Multiple Types of Retinal Neurons Contribute to the AAQ-Mediated Light Response of RGCs

(A) Amacrine cell-mediated synaptic inhibition dominates the RGC light response. MEA recording with antagonists of $GABA_A$ (gabazine; 4 μM), $GABA_C$ (TPMPA; 10 μM), and glycine receptors (strychnine; 10 μM) is shown. Top: Raster plot of RGC spiking. Bottom: Average RGC firing rate.

(B) After blocking inhibition, PI values show a decrease in firing frequency upon switching from darkness to 380 nm light (n = 11 retinas).

(C) Endogenous K^+ channels contribute to the RGC light response. Whole-cell patch clamp recording from an RGC. Currents were evoked by voltage steps from −80 to +40mV in 20mV increments in 380 nm and 500 nm light. Inhibitory GABAergic and glycinergic inputs were blocked as in (A), and excitatory glutamatergic inputs were blocked with DNQX (10 μM) and AP5 (50 μM).

(D) Photoregulation of endogenous K^+ channels evaluated in steady-state I-V curves obtained in 380 and 500 nm light (n = 5 RGCs). Current is normalized to the maximal value at +40mV (380 nm light). Variability among data is expressed as mean ± SEM.

(E) Bipolar cell-mediated synaptic excitation also contributes to the RGC light response. Whole-cell patch clamp recording from an RGC. Blockade of inhibitory synaptic inputs (as in A) and endogenous RGC K^+ channels (as in C) reveals photoregulation of EPSC rate. Note the disappearance of EPSCs after perfusion with glutamate receptor antagonists DNQX (10 μM) and AP5 (50 μM). Holding potential = −60mV.

(F) Average EPSC rate in 380 nm and 500 nm light. Note the significant increase in EPSC rate in 500 nm light ($p < 0.05$, Mann-Whitney test; n = 9 cells). Red symbols show median values and error bars represent 95% confidence intervals.

See also Figure S3.

RGCs implies that a sign-inverting synapse from a laterally-projecting neuron is involved in transmitting information from the center illuminated area to the surround. Amacrine cells are known to form a mutually inhibitory network, making them the likely source of the inhibitory signal.

Spectral Requirements of AAQ-Mediated Light Responses

We determined the optimal wavelength for turning off RGC firing when the AAQ photoswitch is driven from the *cis* to the *trans* configuration. First, a conditioning 380 nm stimulus was used to turn on firing and then we measured suppression of firing in response to test flashes of different wavelengths. We found that 500 nm light is best at suppressing activity (Figure 4A), as expected from previous results (Fortin et al., 2008). To determine which wavelengths are best at triggering firing when AAQ photoisomerizes from *trans* to *cis*, we again applied test flashes of different wavelengths, but to ensure that the photoswitch started maximally in the *trans* configuration, the stimulation protocol began with a reset flash of 500 nm light followed by a period of darkness. We found that the optimal wavelength for stimulating firing was 380 nm under these conditions. However, robust firing could also be activated with 420 or 460 nm light (Figure 4B), and even 500 nm light could trigger an increase in firing frequency if the preceding dark interval was sufficiently long. The history dependence of photoswitching is a consequence of the initial ratio of the *cis* and *trans* photoisomers. Starting with all molecules in the *trans* state, even 500 nm light can increase the fraction of *cis* molecules. Hence, UV light is not essential for eliciting retinal responses. We also found that broad spectrum white light can trigger an increase in firing frequency in RGCs (Figures 4C and 4D).

We measured the absolute light intensity required to photoregulate AAQ-treated retinas from rd1 mice. The threshold intensity required to induce RGC firing was 2.6×10^{15} photons/cm^2/s of 380 nm light (Figure 4E). The RGC firing rate increased progressively with brighter light, up to 10^{17} photons/cm^2/s, but even this intensity did not saturate the response. By comparison, retinas from rd1 mice expressing ChR2 in bipolar cells (Lagali et al., 2008) have RGCs that exhibit a firing threshold of 6×10^{15} photons/cm^2/s.

Restoring Behavioral Light Responses In Vivo with AAQ

Given that AAQ can bestow photosensitivity onto blind retinas ex vivo, we asked whether it can confer light-induced behavior in blind mice in vivo. Although rd1 mice lose all morphologically recognizable rods and cones, a small fraction of cones with altered morphology can survive, allowing correct performance

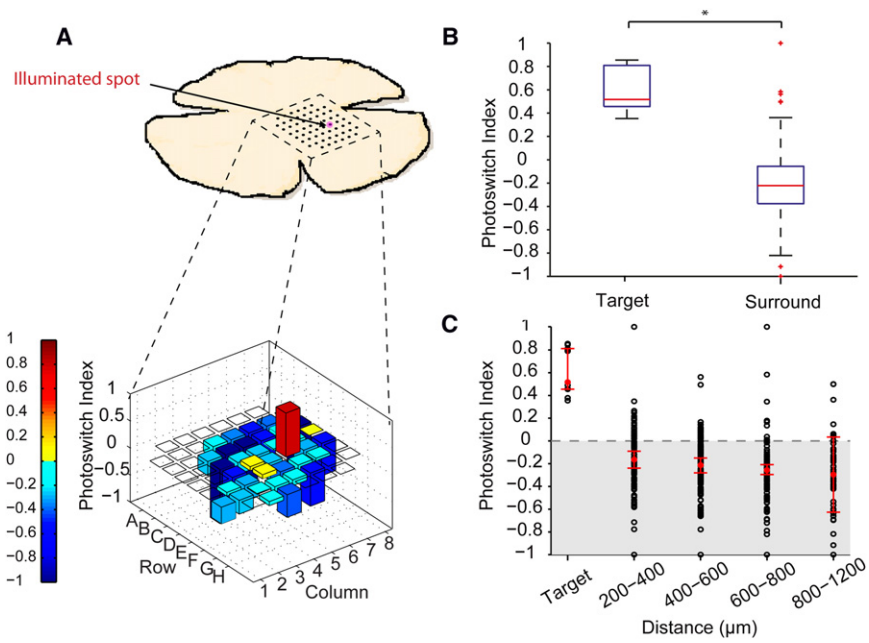

Figure 3. The AAQ-Treated Retina Generates Spatially Precise Light Responses

(A) Targeted illumination of a portion of the retina centered on a single MEA electrode (top). The target (electrode E6) was exposed to 3 s flashes of alternating 380 and 500 nm light. Spot size = 60 μm in radius, inter-electrode spacing = 200 μm. Only the targeted electrode records an increase in RGC firing in response to 380 nm light (bottom). PI values are color-coded (scale at left) and also represented by bar height. The red bar is electrode E6 (PI = 0.812; n = 1 cell), and blue electrodes are the surround (PI = −0.209; n = 56 cells). Empty squares are electrodes on which no action potentials were recorded.

(B) Targeted illumination results from three retinas, displayed in a box plot. PI values for the target and the surround RGCs are significantly different from one another ($p < 0.005$, Mann-Whitney test). Whiskers denote 1.5 times the interquartile range from the 25th and 75th percentile.

(C) Targeted illumination elicits opposite responses in center and surround RGCs (n = 11 cells and n = 385 cells, respectively, from three retinas). PI values of RGCs (open circles) as a function of distance from the target electrode, displayed in 200 μm bins. The red diamonds indicate the median plus or minus the bootstrapped 95% confidence intervals. See Table 1 for values.

of a visual discrimination task under some illumination conditions (Thyagarajan et al., 2010). Rd1 mice also exhibit a pupillary light reflex (PLR), but this behavior is completely absent from rd1 mice lacking melanopsin, the photopigment found in the small percentage (~3%) of RGCs that are intrinsically photosensitive (ipRGCs) (Hattar et al., 2002; Panda et al., 2003). Therefore, we tested the PLR of adult rd1 mice lacking the melanopsin gene (*opn4*$^{-/-}$ *rd1/rd1*) (Panda et al., 2003). After 3 months of age, no PLR could be elicited in any of the mice that we tested, even with the brightest light available (Figure 5A). However, in a subset of these mice (9 out of 25), intravitreal injection of AAQ resulted in a substantial PLR, with a maximal pupillary constriction of ~65% as large as wild-type. Control experiments showed no restoration of the PLR following sham injection of vehicle alone (n = 4; Figure S4). The AAQ-mediated response was attributable to the retina, as direct application of AAQ to the isolated iris in vitro did not produce light-elicited constriction. In the remaining mice, suboptimal intravitreal placement or leakage resulting from puncture damage may have reduced how much AAQ reached the retina, precluding effective photosensitization.

Table 1. Center and Surround RGC Responses under Targeted Illumination

Distance (um)	No. of Cells	Median PI	95% Confidence Interval
Target	11	0.517	0.455 to 0.812
200–400	95	−0.165	−0.239 to −0.090
400–600	143	−0.213	−0.284 to −0.150
600–800	97	−0.256	−0.294 to −0.206
800–1,200	50	−0.296	−0.626 to 0.034

The AAQ-mediated PLR in *opn4*$^{-/-}$ *rd1/rd1* mice could be triggered by photopic irradiance levels normally encountered during daytime, but the PLR threshold was 2 to 3 log units higher than the normal PLR in wild-type mice (Figure 5B). The AAQ-mediated PLR was slower than in wild-type mice (see Movie S1), and AAQ induced some basal pupillary constriction in darkness. Nonetheless, these results show that light responses in AAQ-treated retina can drive brain circuits, leading to a behavioral response that is absent from untreated blind animals.

We next tested whether locomotory light-avoidance behavior (Johnson et al., 2010; Kandel et al., 1987) could be restored in blind *opn4*$^{-/-}$ *rd1/rd1* mice treated with a unilateral intravitreal injection of AAQ. We placed a mouse into a narrow cylindrical transparent tube and recorded behavior with an infrared video camera (Figure 6A). An automated image analysis system was used to detect the mouse and measure how quickly it moved away from the illuminated end of the tube, toward the center. The latency to movement was significantly shorter in light than in darkness in wild-type mice (n = 13, 26 trials, $p < 0.01$) but not in *opn4*$^{-/-}$ *rd1/rd1* mice (n = 7, 14 trials), indicating light avoidance in the wild-type mice but not in the mutant mice. AAQ reinstated the light versus dark latency difference, measured 2 hr after injection (n = 7, 14 trials, $p < 0.02$), indicating restoration of light avoidance. At 24 hr after AAQ injection, there was no difference in latency in light versus darkness, consistent with dissipation of the AAQ. These results indicate that an active light-avoidance behavior can be elicited by AAQ following a single injection into the eye.

Wild-type mice exhibit a decrease in open-field locomotion in response to light, which corresponds to a decrease in exploratory drive (Bourin and Hascoët, 2003). In contrast, rd1 mice

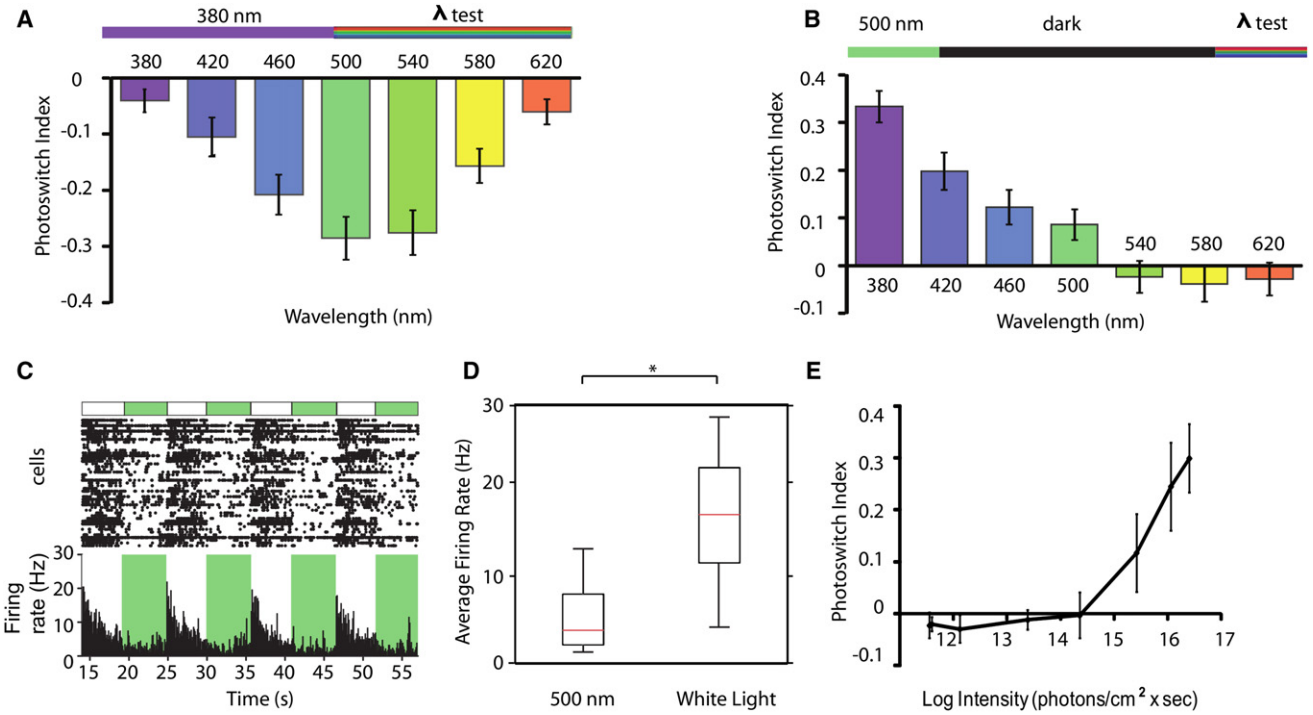

Figure 4. Spectral and Illuminance Sensitivity of AAQ-Mediated Photocontrol of RGC Firing

(A) Spectral sensitivity of light-elicited suppression of RGC firing. Top: Light stimulation protocol. AAQ was first driven into its *cis* configuration with 380 nm light (5 s), and various test wavelengths triggered photoisomerization to the *trans* configuration. Bottom: PI values reveal the effectiveness of different wavelengths in suppressing RGC firing (n = 5 retinas). Error bars represent mean ± SEM.

(B) Spectral sensitivity of light-elicited activation of RGC firing. Top: Light stimulation protocol. AAQ was first driven into its *trans* configuration with 500 nm light (15 s). After an additional dark period (45 s) various test wavelengths triggered photoisomerization to the *cis* configuration. Bottom: PI values reveal the effectiveness of different wavelengths in stimulating RGC firing (n = 5 retinas). For (A) and (B), the PI was measured over the first 1 s after applying the test wavelength. Error bars represent mean ± SEM.

(C) Stimulation of RGC firing in an AAQ-treated retina with white light. Top: Raster plot of spiking from RGCs. Bottom: Average RGC firing rate.

(D) Box plot representation of increased firing rate in white light versus 500 nm. White light significantly increases peak firing rate ($p < 0.05$, Mann-Whitney test, n = 5). Whiskers denote 1.5 times the interquartile range from the 25th and 75th percentile.

(E) Light intensity-response relationship for AAQ-treated *rd1* mouse retinas exposed to different intensities of 380 nm light. Minimum light intensity needed for photoswitching is 2.6×10^{15} photons/cm^2/s. Error bars represent mean ± SEM.

exhibit no change in locomotion over at least a 10 min period of illumination (Lin et al., 2008). In order to determine if AAQ can support light modulated exploratory behavior in rd1 mice, we carried out open field experiments. We placed a mouse into a circular test chamber and monitored movement during 5 min in darkness followed by 5 min in 380 nm light. Figures 7A and 7B show an example of the effect of AAQ on one rd1 mouse (see also Movies S2 and S3). Before AAQ, light had no effect

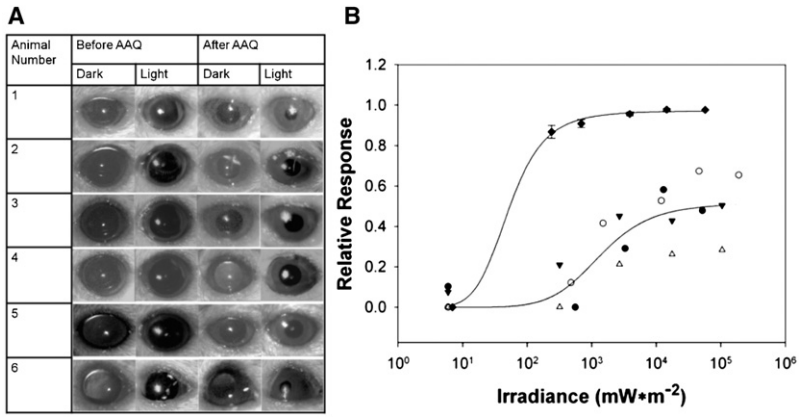

Figure 5. AAQ Restores the Pupillary Light Reflex in Mice Lacking All Retinal Photoreceptors

(A) Pupillary light responses to 5.5×10^4 mW/m^2 white light in *opn4*$^{-/-}$ *rd/rd* mice, before (left) and 3 hr after (right) intravitreal injection of AAQ (1 μl of 80 mM in DMSO). Dark images taken 5 s before light stimulus; light images represent maximal pupillary constriction during 30 s light exposure. Images were taken with an infrared-sensitive camera under infrared illumination.

(B) Irradiance-dependence of pupillary light responses to white light. Irradiance response for wild-type mice (plotted as mean ± STD, n = 5) (◆) and four *opn4*$^{-/-}$ *rd/rd* mice injected with AAQ (plotted individually: ● ○ ▼ Δ). Data were fitted with a three parameter Hill equation.

See also Figure S4 and Movie S1.

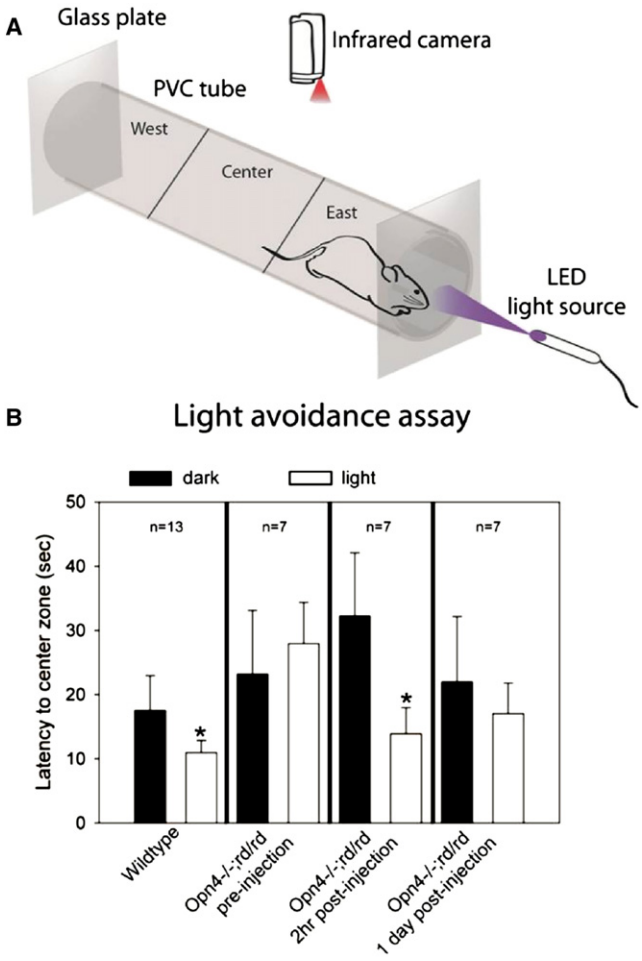

Figure 6. AAQ Restores Active Light Avoidance Behavior in Mice Lacking All Retinal Photoreceptors

(A) Schematic diagram of the locomotory light-avoidance test chamber.

(B) Restoration of light avoidance behavior in *opn4*$^{-/-}$ *rd/rd* mice following AAQ injection. Bars represent mean latency of movement from the "East" to the "Center" third of the tube (plotted as ± STD).

on the movement trajectory (Figure 7A) or total distance traveled (Figure 7B). After AAQ, light caused an almost immediate decrease in exploratory behavior, quantified as diminished distance traveled. Average data from eight rd1 mice showed no light versus dark difference in movement before AAQ (Figure 7C). However, after AAQ, there was a decrease in movement that occurred within 30 s of light onset. This decrease was sustained throughout the illumination period. Before AAQ, there was no statistically significantly change in the speed of locomotion in light as compared to darkness (Figure 7D), but after AAQ injection, light caused a significant 40% slowing of locomotion. Sham injections with vehicle alone elicited no significant change in light modulated behavior ($n = 4$, $p > 0.6$). Further analysis of the eight mice showed that seven of them exhibited significant light-evoked slowing of locomotion after AAQ injection (Figure 7E).

After termination of the behavioral test, mice were sacrificed and retinas were placed on the MEA for electrophysiological analysis. In five cases, we successfully obtained MEA recordings and were able to directly compare the AAQ-mediated photosensitization of the retina ex vivo with the behavioral responses in vivo. The one mouse that failed to exhibit light-modulated behavior (mouse A in Figures 7E and 7F) also failed to exhibit light-sensitive retinal responses. For all of the other four mice, light-elicited behavior corresponded with a light-elicited change in firing rate.

Rd1 mice possess ipRGCs, which should respond to the light used in this behavioral test. However, previous studies (Lin et al., 2008) show that ipRGCs do not mediate short-term light-elicited changes in exploratory behavior. Moreover, in our open field experiments, mice exhibited no light-modulated behavior prior to AAQ injections, confirming that alone, the ipRGCs are not sufficient to evoke this behavior.

DISCUSSION

The ultimate goal of vision restoration research is to recreate as closely as possible the activity of the entire population of RGCs in response to a natural visual scene. Since only a small fraction of RGCs are intrisically light-sensitive (Ecker et al., 2010; Panda et al., 2003), photosensitivity must be conferred artificially by directly or indirectly making the neurons sensitive to light. Ideally, the kinetics and absolute sensitivity to light should be equivalent to natural RGC responses. The healthy retina has a remarkably broad operating range owing to light-adaptation mechanisms, so the artificial system should include gain adjustment and range extension capabilities. Ideally, the system would replicate normal encoding of contrast and color and highlight movement, with certain RGCs being directionally selective. All of this should be accomplished with a minimally invasive and safe technology. To date, no restorative technology is close to meeting these criteria, but new developments are providing reason for optimism.

Broadly, three approaches have been suggested for restoring visual function to the eye in the absence of rods and cones: optoelectronic engineering with retinal chip prosthetics; genetic engineering with viral-mediated delivery of optogenetic tools; and cellular engineering, with rod or cone progenitors differentiated from stem cells in vitro. We now describe a fourth approach: photochemical engineering with a small molecule photoswitch. The following functional considerations suggest that the photoswitch approach compares favorably with other methods for restoring visual function and offers some practical advantages.

Kinetics

AAQ-mediated retinal light responses are rapid. MEA recordings show that the median response latency of RGC spiking is 45 ms in the AAQ-treated rd1 mouse retina, compared to ~50 ms (Farrow and Masland, 2011) to several hundred ms (Carcieri et al., 2003) for photopic light responses from RGCs in wild-type retina. Retinal chips electrically stimulate RGCs directly, and therefore can elicit spikes with latencies of several milliseconds. For optogenetic tools, depending on which retinal cell type expresses the tool, the response latency of RGCs ranges from several milliseconds to 150 ms (Bi et al., 2006; Busskamp et al., 2010; Lagali et al., 2008). Stem cell-based therapies would

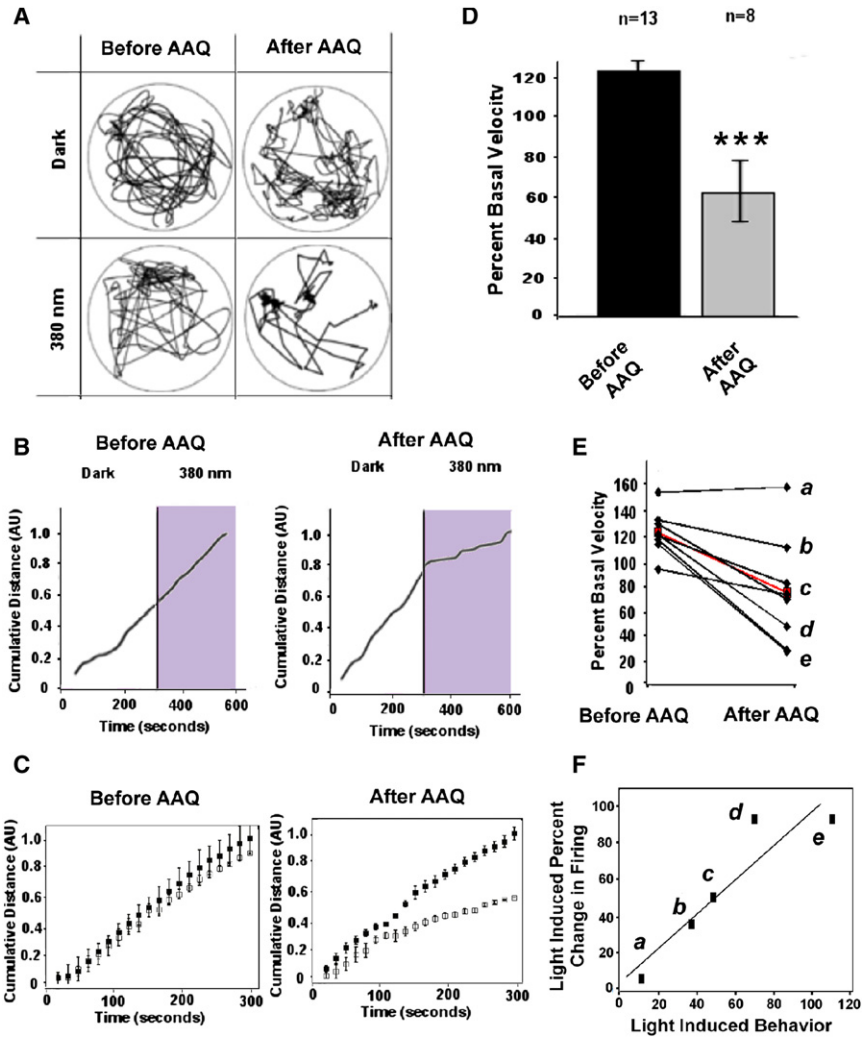

Figure 7. AAQ Restores Light-Modulated Locomotor Behavior in an Open-Field Test

(A) Paths traveled by an rd1 mouse before and after injection with AAQ in darkness and with 380 nm illumination.

(B) Cumulative distance traveled by the mouse in darkness and in 380 nm light, before and after AAQ.

(C) Average cumulative distance traveled of all mice in darkness and 380 nm light, before and after AAQ. Closed squares represent time spent in darkness while open squares represent time spent in 380 nm light. (mean ± SEM, n = 8).

(D) Mean locomotory velocity in light normalized to basal velocity in darkness. Velocity decreases significantly in light (n = 8, $p < 0.0006$).

(E) Light evoked change in the velocity of each of the eight mice before and after AAQ. The red line shows the mean light evoked change before and after AAQ.

(F) Light-induced behavior is correlated with the light-induced change in firing rate. Data were from the five mice for which both in vivo behavioral measurement and ex vivo retinal MEA recordings were obtained (as labeled a–e in panel E). The light-induced percent change in firing rate was calculated from the aggregate light response for all units recorded with the MEA upon switching from darkness to 380 nm light. The light-induced behavior represents percent change in velocity upon switching from darkness to 380 nm light.

See also Movies S2 and S3.

presumably restore wild-type kinetics, assuming the differentiated rods and cones have full function.

Sensitivity

MEA recordings in vitro and PLR measurements in vivo indicate that the AAQ-treated rd1 mouse retina responds under bright photopic conditions, comparable to levels achieved in natural outdoor illumination. This is similar to light sensitivity conferred onto RGCs by optogenetic tools (Bi et al., 2006; Thyagarajan et al., 2010). Exogenous expression of NpHR in cone remnants can result in higher light sensitivity (Busskamp et al., 2010). However, it is unclear whether many patients with advanced RP have sufficient cone remnants to allow this to be a broadly applicable approach (Milam et al., 1998). High sensitivity can also be conferred by exogenously expressing melanopsin in RGCs that are not normally light-sensitive (Lin et al., 2008), but the responses are variable and slow (on the order of seconds). Stem cell-based therapies in theory might recapitulate the wild-type sensitivity of rods and cones. However, the human retina normally contains >100,000,000 rods and cones, and whether a significant fraction can be restored with stem cells remains unclear.

Spatial Resolution and Extent of Retinal Functional Restoration

AAQ-mediated retinal responses have a high spatial resolution. Our spot illumination experiments places a 100 μm radius upper limit on the AAQ-mediated receptive field size. Amacrine cells, which predominate in driving RGC responses, can project over several hundred μm, but mutual inhibition between these cells presumably spatially constrains RGC responses to a smaller area. Because AAQ is a diffusible small molecule, in principle it should reach the entire retina and confer light sensitivity on all RGCs. In practice, we observed robust light responses in almost all RGCs when AAQ was applied in vitro, but intravitreal injections in vivo were less effective, with only 25%–36% of injections resulting in behavioral responses to light. Drug delivery via intravitreal injections in mice can be unreliable because of the very small vitreal volume (20 μl), which is 250-fold less than the vitreal volume of the human eye (5.5 ml). Further experiments using animals with larger vitreal volumes are needed to better test and optimize the effectiveness of intravitreal AAQ administration.

In contrast to the relatively high spatial resolution that could be conferred by AAQ, the spatial resolution of a retinal chip is limited by the relatively large size of the stimulating electrodes and the spread of current emanating from each electrode. While the

healthy human retina contains ~1.2 million RGCs, current retinal chips have 16–64 electrodes spaced 100–200 μm apart (Winter et al., 2007). Chips with electrodes more densely packed exhibit crosstalk between electrodes, limiting their effectiveness. At present, the highest resolution that could be provided by retinal chip stimulation is several orders of magnitude lower than the theoretical limits imposed by RGC density in the macula, the region crucial for high-acuity vision. The area of RGC stimulation is limited by the physical size of the chip implant, which typically covers only the central 20 degrees of vision in the macula (Chader et al., 2009). Larger chips are possible, but there are challenges in power delivery and achieving stable adherence to the retina.

Similar to photoswitches, the spatial resolution conferred by optogenetic tools is defined by the size of the cell type targeted for expressing a given light-activated protein. In principle, the smaller the cell type and the more densely they are packed together, the higher the spatial resolution. In practice, viral transduction with current vectors has resulted in expression of optogenetic tools in a minority of targeted cells (e.g., ~5% of bipolar cells in mice [Lagali et al., 2008] and 5%–10% of RGCs in marmosets [Ivanova et al., 2010]), but it is possible that new viral vectors will be developed that improve transduction efficiency (Vandenberghe et al., 2011). Viral transduction of NpHR has resulted in more efficient transduction (50%–75%) of remnant cones in blind mice (Busskamp et al., 2010), but this approach is only appropriate for the few patients thought to possess remnant cones. Viral transduction of cones requires subretinal injection, which involves local detachment of a portion of the retina from the underlying retinal pigment epithelium. Effective viral gene transfer is limited to the detached area (Hauswirth et al., 2008).

Stem cell approaches offer the potential for greater spatial resolution, but this is dependent on having a high density of differentiated photoreceptor cells that form functional and anatomically correct synapses with appropriate retinal neuron partners, and at present, only a very low density of cells has been achieved (Lamba et al., 2009).

ON and OFF Retinal Output Channels

Optogenetic tools have the advantage of being genetically-targetable to particular types of neurons to generate the appropriate stimulation or inhibition of firing, for example to ON- or OFF-RGCs (Busskamp et al., 2010; Lagali et al., 2008). Moreover, ChR2 and NpHR can be co-expressed in the same RGC and trafficked to different compartments to restore antagonistic center-surround responses (Greenberg et al., 2011). In contrast, all RGCs in AAQ-treated retina respond with the same polarity light response. While this pattern of responsiveness is different than the normal retina, it may not preclude a useful visual experience. Behavioral studies in primates demonstrate that the selective pharmacological blockade of ON neurons does not severely impair recognition of shapes or detection of light decrements (Schiller et al., 1986). Moreover, in RP patients, electronic retinal prosthetics can restore shape recognition, even though the devices stimulate ON- and OFF-RGCs indiscriminately (Sekirnjak et al., 2009). Hence, while two channels of visual information flow are important for normal vision, simultaneous activation of ON- and OFF-pathways is sufficient for visual perception. AAQ treatment enables RGCs surrounding an illuminated area to respond with the opposite polarity to those in the center. Since all RGCs respond with the same polarity light response to full-field illumination (Figure 1A), the opposite center versus surround responses to spot illumination suggests that inhibitory neurons that project laterally invert the sign of the response. It seems likely that the opposite center versus surround response would enhance perception of spatial contrast and facilitate edge detection in downstream visual regions of the brain. But ultimately, the evaluation of the quality of images produced by photoswitch activation of retinal cells will require study in primates or human patients.

Spectral Sensitivity

In AAQ-treated retinas, RGCs respond most strongly to short wavelength light, consistent with the photochemical properties of the molecule (Fortin et al., 2008). Although 380 nm light is optimal for enhancing firing frequency, longer wavelengths (up to 500 nm) can still generate excitatory light responses, reflecting the spectral range of *trans* to *cis* azobenzene photoisomerization. This is important, because unlike in the mouse, the human lens minimally transmits 380 nm light (Kessel et al., 2010). Newly-developed red-shifted azobenzene derivatives allow K^+ channel regulation with even longer wavelengths of light and chemical modification of the azobenzene moiety results in compounds with improved quantum efficiency (Mourot et al., 2011). Ideally, second-generation AAQ derivatives would enable photostimulation of the retina with intensities and wavelengths experienced during normal photopic vision. Alternatively, a head-mounted optoelectronic visual aid (Degenaar et al., 2009) designed to intensify and transform the palette of visual scenes to a blue-shifted wavelength could enhance the effectiveness of AAQ and related agents. Such a device might also allow switching of individual RGCs ON and OFF by rapid modulation of shorter- and longer-wavelength light.

Except for some of the optogenetic tools, the other vision restoration methods pose no particular spectral challenges. NpHR and ChR2 respond optimally to 580 and 470 nm light, respectively (Nagel et al., 2003; Zhang et al., 2007), but newly discovered red-shifted homologs (Govorunova et al., 2011) expand the toolkit for potential use for photosensitizing retinal neurons. Since they are driven by images captured by an external camera, retinal chip prosthetics can be engineered to operate over the entire visual spectrum. Similarly, assuming stem cell-derived photoreceptors express the full complement of cone opsins, these should be responsive to a broad range of wavelengths.

Invasiveness, Safety, and Reversibility

The phototswitch approach has the advantage of being relatively noninvasive and readily reversible. We envision photoswitch molecules being administered therapeutically by intravitreal injection, a safe and frequent procedure for treating macular degeneration with anti-vasoproliferative agents. Because AAQ photosensitization dissipates within 24 hr, it may be possible to titrate the most effective dose with repeated intravitreal injections. The reversibility of AAQ will allow for "upgrades" as newer

agents become available, perhaps with improved spectral or kinetic properties. Longer-term therapy would require an extended release formulation. We estimate that a several month supply of AAQ could be packaged into an intravitreal device like those currently used for long-term steroid treatment of ocular inflammation (London et al., 2011).

In contrast, retinal chip prosthetics require invasive intraocular surgery. Optogenetic treatment of remnant cones and stem cell therapy both require subretinal injection, a risky procedure that begins with iatrogenic retinal detachment, which could further damage the retina. These three approaches are essentially irreversible. Should they produce undesired effects (such as chronic photophobia or disturbing visual sensations) there is no ready means for reversal of either stem cell implantation or gene therapy, and removal of chip prosthetics would require additional significant surgery.

Both retinal chip prosthetics and human gene replacement therapy have received investigational new device/drug status and have been tested in human patients under research protocols (Ahuja et al., 2011; Benav et al., 2010) without significant toxicity. However, microbial optogenetic tools would require trans-species gene therapy, which is unprecedented. Viral gene expression in the eye can elicit late-onset inflammation, indicating an immune reaction (Beltran et al., 2010). Because the unitary conductance of ChR2 and NpHR is quite small (Feldbauer et al., 2009; Sjulson and Miesenböck, 2008; Zhang et al., 2007), photosensitivity requires very high levels of exogenous expression, raising concerns about an immune response to the microbially-derived protein or cytotoxicity. While long-term safety of AAQ or similar compounds will require toxicology studies, to date, we have not seen acute toxicity of AAQ on neural function in vitro (Fortin et al., 2008) or in vivo (Figure S2). The pathway for evaluating photoswitch compounds for toxicity is straightforward and will mirror those that have been followed for other approved, intravitreal agents.

Finally, in addition to its potential clinical use, AAQ has utility as a scientific tool for understanding normal retinal function and development. Using AAQ, the firing activity of single cells or small regions of the retina can be controlled with high temporal and spatial resolution. This may be useful for better understanding information processing by the retina and for studying developmental plasticity in animals before rods and cones are functional (Huberman et al., 2008). AAQ-mediated photocontrol of retinal neurons also provides a unique way to investigate circuit remodeling after the rods and cones have degenerated in mouse models of RP (Marc et al., 2003).

EXPERIMENTAL PROCEDURES

Animals

Wild-type mice (C57BL/6J strain, Jackson Laboratories) and homozygous rd1 mice (C3H/HeJ strain, Charles River Laboratories) >3 months old were used for the experiments. All animal use procedures were approved by the UC Berkeley or University of Washington Institutional Animal Care and Use Committee (see Supplemental Experimental Procedures).

Electrophysiology and Pharmacology

Mouse retinas were dissected and kept in physiological saline at 36°C containing (in mM) 119 NaCl, 2.5 KCl, 1 KH_2PO_4, 1.3 $MgCl_2$, 2.5 $CaCl_2$, 26.2 $NaHCO_3$, and 20 D-glucose, aerated with 95% O_2/5% CO_2. For extracellular recording, the retina was placed ganglion cell layer down onto a multielectrode array system (model number MEA 1060-2-BC, Multi-Channel Systems).

The MEA electrodes were 30 μm in diameter and arranged on an 8 × 8 rectangular grid. Extracellular spikes were high-pass filtered at 200 Hz and digitized at 20 kHz. A spike threshold of 4SD was set for each channel. Typically, each electrode recorded spikes from one to three RGCs. Principal component analysis of spike waveforms was used for sorting spikes generated by individual cells (Offline Sorter; Plexon). Only cells with interspike intervals of <1 ms were included in the analysis.

Borosilicate glass electrodes of 6–11 MΩ were used for whole-cell voltage-clamp recordings. Current records were low-pass filtered at 2 kHz. For measuring voltage-gated K^+ currents, electrodes contained (in mM) 98.3 K^+ gluconate, 1.7 KCl, 0.6 EGTA, 5 $MgCl_2$, 40 HEPES, 2 ATP-Na, and 0.3 GTP-Na (pH = 7.25). For recording glutamatergic EPSCs, electrodes contained (in mM) 125 Cs^+ sulfate, 10 TEA-Cl, 5 EGTA, 0.85 $MgCl_2$, 10 HEPES, 2 QX-314, and 4 ATP-Na_2 (pH = 7.25). Neurotransmitter receptor antagonists were used to evaluate synaptic contributions of different retinal neurons to RGC light responses (see Supplemental Experimental Procedures).

Light Stimulation

In MEA recordings, we used a 100 W mercury arc lamp filtered through 380 or 500 nm narrow-pass filters (Chroma, Inc.) and switched wavelengths with an electronically-controlled shutter and filter wheel (SmartShutter, Sutter Instruments). Unless otherwise indicated, the standard incident light intensity at the retina was 13.4 mW/cm^2 (2.56 × 10^{16} photons/cm^2/s) for 380 nm and 11.0 mW/cm^2 (2.77 × 10^{16} photons/cm^2/s) for 500 nm.

PLR Measurement

Mice were sedated with an intraperitoneal injection of ketamine (6.7mg/ml) and xylazine (0.45 mg/ml) in saline. A glass micropipette was inserted through the sclera into the vitreous cavity to inject a 1 μl bolus of AAQ (80 mM in a saline solution containing 40% DMSO).

Videos of pupillary light responses of mice were recorded before and 3 hr after AAQ injection. White light was derived from halogen dissecting lamp, and intensity was controlled with neutral density filters. Animals were dark-adapted for at least 20 min prior to testing. An infrared (IR) illuminator and video camera (focused 15 cm from the objective) was used to measure pupil dilation, as described (Van Gelder, 2005).

Locomotory Light Avoidance

Wild-type or *opn4*$^{-/-}$ *rd/rd* mice injected with 80 mM AAQ were dark-adapted and placed into a transparent tube. The tube was illuminated with IR light and mouse movement was recorded with an IR video camera and stored for offline analysis. During testing, the face of the mouse was illuminated with 385 nm light (log irradiance 15.7) and at 5 s intervals flashes of 480 nm light (log irradiance 15.2) were superimposed. For each mouse, we recorded position in the tube preinjection, and 2 hr and 24 hr postinjection. Analysis was conducted with automated image-analysis software.

Open-Field Test

Rd1 mice were placed in a 190 mm × 100 mm circular UV-transparent chamber. The chamber was surrounded by six panels of 380 nm LEDs (Roithner Laserteknik), providing uniform illumination with a light intensity of ~7 mW/cm^2.

The mice were dark-adapted in their cages for 1 hr prior to each experiment. The mice were placed in the experimental chamber and allowed to acclimate for 5 min. The behavior was then recorded using an IR sensitive video camera (Logitech C310) for 5 min in darkness under IR illumination. After 5 min, the chamber was illuminated by the 380 nm LEDs, and behavior was monitored for an additional 5 min. The apparatus was cleaned and thoroughly dried prior to each experiment.

After the open-field test, each mouse was given an intravitreal injection of AAQ (20 mM AAQ, 9:1 saline: DMSO) and were allowed to recover for ~6 hr on a heating pad with open access to food and water in their cage located in the dark room followed by a second round of behavioral testing. The videos were analyzed utilizing motion tracking video analysis software (Tracker) in

order to quantify the average velocity of the mice, the trajectory of motion throughout the test, and the total distance traveled.

Data Analysis and Statistics

Light-elicited changes in firing rate during test flashes were normalized with respect to initial firing rate and expressed as a PI, defined as follows: PI = (test firing rate – initial firing rate) / (test firing rate + initial firing rate).

Relative pupillary light responses were calculated as 1 – (pupil area minimum during thirty seconds of the light stimulus) / (pupil area minimum during five seconds preceding the stimulus). Relative response data for wild-type and *opn4*$^{-}$/$^{-}$ *rd/rd* mice were fitted with a three parameter Hill equation (SigmaPlot, Systat Software, Inc.). Data are expressed as mean ± SEM, unless otherwise indicated. The p values for open-field experiments were calculated using the two tailed unpaired Students t test.

Latencies were calculated for every cell with a PI greater than 0.011, the upper median confidence interval PI of our control experiments (n = 13 retinas; n = 409 cells). For each cell, firing rate was averaged over the first two light periods (dark and 380 nm light), with a 10 ms bin size. Basal firing rate was calculated from the upper median confidence interval in 500 nm light. Response latency was then calculated as the time difference between the onset of 380 nm light and the first bin with a firing rate greater than the cell's basal activity. The median response latency was 45 ms (n = 10 retinas; n = 368 cells).

All statistics were performed with MATLAB (Mathworks) algorithms. Distributions were first tested for normality using the Shapiro-Wilk test. For non-normal distributions, the Wilcoxon rank sum test was used for pairwise comparisons. The 95% confidence intervals for medians were generated by resampling the original distributions and applying the bias-corrected percentile method (Efron and Tibshirani, 1986). Results with $p < 0.05$ were considered significant.

For all box plots, box limits represent the 25th and 75th percentile, respectively. The red line represents the median and whiskers denote 1.5 times the interquartile range from the limits of the box. Outliers are marked by red + signs.

SUPPLEMENTAL INFORMATION

Supplemental Information includes four figures, two tables, Supplemental Experimental Procedures, and three movies and can be found with this article online at http://dx.doi.org/10.1016/j.neuron.2012.05.022.

ACKNOWLEDGMENTS

We thank A. Anishchenko and J. Elstrott for helpful comments and discussions; Trevor Lee, Andrew Noblet, R. Montpetit, T. Lamprecht, and X. Qiu for technical and experimental assistance; and J. Flannery and K. Greenberg for valuable suggestions. This work was supported by the National Eye Institute (NEI), which provided research Grant EY018957 to R.H.K., Core Grant P30 EY003176 to R.H.K., and Core Grant P30 EY001730 to R.V.G. This work was also supported by Beckman Foundation for Macular Research (R.H.K.) and a Research to Prevent Blindness award to Y.S. and R.V.G. and an Ezell Fellowship to A.P. The NEI also funded the Nanomedicine Development Center (PN2 EY018241), which supported this interdisciplinary project. R.H.K. and D.T. are SAB members and consultants of Photoswitch Bioscience, Inc., which is developing commercial uses for chemical photoswitches. A.P., J.L., I.T., J.N., Y.S., T.H., I.D.K., and K.B. conducted the in vitro and in vivo experiments. D.T. designed and synthesized chemical reagents. R.H.K. and R.V.G. coordinated the research and wrote the manuscript. R.H.K. initiated the research and supervised the program.

Accepted: April 30, 2012
Published: July 25, 2012

REFERENCES

Ahuja, A.K., Dorn, J.D., Caspi, A., McMahon, M.J., Dagnelie, G., Dacruz, L., Stanga, P., Humayun, M.S., and Greenberg, R.J.; Argus II Study Group. (2011). Blind subjects implanted with the Argus II retinal prosthesis are able to improve performance in a spatial-motor task. Br. J. Ophthalmol. *95*, 539–543.

Banghart, M.R., Mourot, A., Fortin, D.L., Yao, J.Z., Kramer, R.H., and Trauner, D. (2009). Photochromic blockers of voltage-gated potassium channels. Angew. Chem. Int. Ed. Engl. *48*, 9097–9101.

Beltran, W.A., Boye, S.L., Boye, S.E., Chiodo, V.A., Lewin, A.S., Hauswirth, W.W., and Aguirre, G.D. (2010). rAAV2/5 gene-targeting to rods:dose-dependent efficiency and complications associated with different promoters. Gene Ther. *17*, 1162–1174.

Benav, H., Bartz-Schmidt, K.U., Besch, D., Bruckmann, A., Gekeler, F., Greppmaier, U., Harscher, A., Kibbel, S., Kusnyerik, A., Peters, T., et al. (2010). Restoration of useful vision up to letter recognition capabilities using subretinal microphotodiodes. In Engineering in Medicine and Biology Society (EMBC), 2010 Annual International Conference of the IEEE, pp. 5919–5922.

Bi, A., Cui, J., Ma, Y.P., Olshevskaya, E., Pu, M., Dizhoor, A.M., and Pan, Z.H. (2006). Ectopic expression of a microbial-type rhodopsin restores visual responses in mice with photoreceptor degeneration. Neuron *50*, 23–33.

Bourin, M., and Hascoët, M. (2003). The mouse light/dark box test. Eur. J. Pharmacol. *463*, 55–65.

Busskamp, V., Duebel, J., Balya, D., Fradot, M., Viney, T.J., Siegert, S., Groner, A.C., Cabuy, E., Forster, V., Seeliger, M., et al. (2010). Genetic reactivation of cone photoreceptors restores visual responses in retinitis pigmentosa. Science *329*, 413–417.

Caporale, N., Kolstad, K.D., Lee, T., Tochitsky, I., Dalkara, D., Trauner, D., Kramer, R., Dan, Y., Isacoff, E.Y., and Flannery, J.G. (2011). LiGluR restores visual responses in rodent models of inherited blindness. Mol. Ther. *19*, 1212–1219.

Carcieri, S.M., Jacobs, A.L., and Nirenberg, S. (2003). Classification of retinal ganglion cells: a statistical approach. J. Neurophysiol. *90*, 1704–1713.

Chader, G.J., Weiland, J., and Humayun, M.S. (2009). Artificial vision: needs, functioning, and testing of a retinal electronic prosthesis. Prog. Brain Res. *175*, 317–332.

Chaudhry, G.R., Fecek, C., Lai, M.M., Wu, W.C., Chang, M., Vasquez, A., Pasierb, M., and Trese, M.T. (2009). Fate of embryonic stem cell derivatives implanted into the vitreous of a slow retinal degenerative mouse model. Stem Cells Dev. *18*, 247–258.

Degenaar, P., Grossman, N., Memon, M.A., Burrone, J., Dawson, M., Drakakis, E., Neil, M., and Nikolic, K. (2009). Optobionic vision—a new genetically enhanced light on retinal prosthesis. J. Neural Eng. *6*, 035007.

Ecker, J.L., Dumitrescu, O.N., Wong, K.Y., Alam, N.M., Chen, S.-K., LeGates, T., Renna, J.M., Prusky, G.T., Berson, D.M., and Hattar, S. (2010). Melanopsin-expressing retinal ganglion-cell photoreceptors: cellular diversity and role in pattern vision. Neuron *67*, 49–60.

Efron, B., and Tibshirani, R. (1986). Bootstrap methods for standard errors, confidence intervals, and other measures of statistical accuracy. Stat. Sci. *1*, 54–75.

Farrow, K., and Masland, R.H. (2011). Physiological clustering of visual channels in the mouse retina. J. Neurophysiol. *105*, 1516–1530.

Feldbauer, K., Zimmermann, D., Pintschovius, V., Spitz, J., Bamann, C., and Bamberg, E. (2009). Channelrhodopsin-2 is a leaky proton pump. Proc. Natl. Acad. Sci. USA *106*, 12317–12322.

Fortin, D.L., Banghart, M.R., Dunn, T.W., Borges, K., Wagenaar, D.A., Gaudry, Q., Karakossian, M.H., Otis, T.S., Kristan, W.B., Trauner, D., and Kramer, R.H. (2008). Photochemical control of endogenous ion channels and cellular excitability. Nat. Methods *5*, 331–338.

Gerding, H., Benner, F.P., and Taneri, S. (2007). Experimental implantation of epiretinal retina implants (EPI-RET) with an IOL-type receiver unit. J. Neural Eng. *4*, S38–S49.

Govorunova, E.G., Spudich, E.N., Lane, C.E., Sineshchekov, O.A., and Spudich, J.L. (2011). New channelrhodopsin with a red-shifted spectrum and rapid kinetics from Mesostigma viride. MBio *2*, e00115–e11.

Greenberg, K.P., Pham, A., and Werblin, F.S. (2011). Differential targeting of optical neuromodulators to ganglion cell soma and dendrites allows dynamic control of center-surround antagonism. Neuron *69*, 713–720.

Hattar, S., Liao, H.W., Takao, M., Berson, D.M., and Yau, K.W. (2002). Melanopsin-containing retinal ganglion cells: architecture, projections, and intrinsic photosensitivity. Science *295*, 1065–1070.

Hauswirth, W.W., Aleman, T.S., Kaushal, S., Cideciyan, A.V., Schwartz, S.B., Wang, L.L., Conlon, T.J., Boye, S.L., Flotte, T.R., Byrne, B.J., and Jacobson, S.G. (2008). Treatment of leber congenital amaurosis due to RPE65 mutations by ocular subretinal injection of adeno-associated virus gene vector: short-term results of a phase I trial. Hum. Gene Ther. *19*, 979–990.

Huberman, A.D., Feller, M.B., and Chapman, B. (2008). Mechanisms underlying development of visual maps and receptive fields. Annu. Rev. Neurosci. *31*, 479–509.

Humayun, M.S., Weiland, J.D., Fujii, G.Y., Greenberg, R., Williamson, R., Little, J., Mech, B., Cimmarusti, V., Van Boemel, G., Dagnelie, G., and de Juan, E. (2003). Visual perception in a blind subject with a chronic microelectronic retinal prosthesis. Vision Res. *43*, 2573–2581.

Ivanova, E., Hwang, G.S., Pan, Z.H., and Troilo, D. (2010). Evaluation of AAV-mediated expression of Chop2-GFP in the marmoset retina. Invest. Ophthalmol. Vis. Sci. *51*, 5288–5296.

Jiménez, A.J., García-Fernández, J.M., González, B., and Foster, R.G. (1996). The spatio-temporal pattern of photoreceptor degeneration in the aged rd/rd mouse retina. Cell Tissue Res. *284*, 193–202.

Johnson, J., Wu, V., Donovan, M., Majumdar, S., Rentería, R.C., Porco, T., Van Gelder, R.N., and Copenhagen, D.R. (2010). Melanopsin-dependent light avoidance in neonatal mice. Proc. Natl. Acad. Sci. USA *107*, 17374–17378.

Kandel, G., Bedell, H., Walker, R., and Wolf, B. (1987). Negative phototaxis in pigmented, albinotic and RCS rat pups measured with a new technique. Vision Sci. *1*, 357–366.

Kessel, L., Lundeman, J.H., Herbst, K., Andersen, T.V., and Larsen, M. (2010). Age-related changes in the transmission properties of the human lens and their relevance to circadian entrainment. J. Cataract Refract. Surg. *36*, 308–312.

Lagali, P.S., Balya, D., Awatramani, G.B., Münch, T.A., Kim, D.S., Busskamp, V., Cepko, C.L., and Roska, B. (2008). Light-activated channels targeted to ON bipolar cells restore visual function in retinal degeneration. Nat. Neurosci. *11*, 667–675.

Lamba, D.A., Gust, J., and Reh, T.A. (2009). Transplantation of human embryonic stem cell-derived photoreceptors restores some visual function in Crx-deficient mice. Cell Stem Cell *4*, 73–79.

Lamba, D.A., Karl, M.O., Ware, C.B., and Reh, T.A. (2006). Efficient generation of retinal progenitor cells from human embryonic stem cells. Proc. Natl. Acad. Sci. USA *103*, 12769–12774.

Lin, B., Koizumi, A., Tanaka, N., Panda, S., and Masland, R.H. (2008). Restoration of visual function in retinal degeneration mice by ectopic expression of melanopsin. Proc. Natl. Acad. Sci. USA *105*, 16009–16014.

London, N.J., Chiang, A., and Haller, J.A. (2011). The dexamethasone drug delivery system: indications and evidence. Adv. Ther. *28*, 351–366.

Marc, R.E., Jones, B.W., Watt, C.B., and Strettoi, E. (2003). Neural remodeling in retinal degeneration. Prog. Retin. Eye Res. *22*, 607–655.

Meister, M., Pine, J., and Baylor, D.A. (1994). Multi-neuronal signals from the retina: acquisition and analysis. J. Neurosci. Methods *51*, 95–106.

Milam, A.H., Li, Z.Y., and Fariss, R.N. (1998). Histopathology of the human retina in retinitis pigmentosa. Prog. Retin. Eye Res. *17*, 175–205.

Mourot, A., Kienzler, M.A., Banghart, M.R., Fehrentz, T., Huber, F.M.E., Stein, M., Kramer, R.H., and Trauner, D. (2011). Tuning photochromic ion channel blockers. ACS Chemical Neuroscience, in press.

Nagel, G., Szellas, T., Huhn, W., Kateriya, S., Adeishvili, N., Berthold, P., Ollig, D., Hegemann, P., and Bamberg, E. (2003). Channelrhodopsin-2, a directly light-gated cation-selective membrane channel. Proc. Natl. Acad. Sci. USA *100*, 13940–13945.

Panda, S., Provencio, I., Tu, D.C., Pires, S.S., Rollag, M.D., Castrucci, A.M., Pletcher, M.T., Sato, T.K., Wiltshire, T., Andahazy, M., et al. (2003). Melanopsin is required for non-image-forming photic responses in blind mice. Science *301*, 525–527.

Punzo, C., and Cepko, C. (2007). Cellular responses to photoreceptor death in the rd1 mouse model of retinal degeneration. Invest. Ophthalmol. Vis. Sci. *48*, 849–857.

Sancho-Pelluz, J., Arango-Gonzalez, B., Kustermann, S., Romero, F.J., van Veen, T., Zrenner, E., Ekström, P., and Paquet-Durand, F. (2008). Photoreceptor cell death mechanisms in inherited retinal degeneration. Mol. Neurobiol. *38*, 253–269.

Schiller, P.H., Sandell, J.H., and Maunsell, J.H. (1986). Functions of the ON and OFF channels of the visual system. Nature *322*, 824–825.

Sekirnjak, C., Hulse, C., Jepson, L.H., Hottowy, P., Sher, A., Dabrowski, W., Litke, A.M., and Chichilnisky, E.J. (2009). Loss of responses to visual but not electrical stimulation in ganglion cells of rats with severe photoreceptor degeneration. J. Neurophysiol. *102*, 3260–3269.

Shire, D.B., Kelly, S.K., Chen, J., Doyle, P., Gingerich, M.D., Cogan, S.F., Drohan, W.A., Mendoza, O., Theogarajan, L., Wyatt, J.L., and Rizzo, J.F. (2009). Development and implantation of a minimally invasive wireless subretinal neurostimulator. IEEE Trans. Biomed. Eng. *56*, 2502–2511.

Sjulson, L., and Miesenböck, G. (2008). Photocontrol of neural activity: biophysical mechanisms and performance in vivo. Chem. Rev. *108*, 1588–1602.

Strettoi, E., and Pignatelli, V. (2000). Modifications of retinal neurons in a mouse model of retinitis pigmentosa. Proc. Natl. Acad. Sci. USA *97*, 11020–11025.

Thyagarajan, S., van Wyk, M., Lehmann, K., Löwel, S., Feng, G., and Wässle, H. (2010). Visual function in mice with photoreceptor degeneration and transgenic expression of channelrhodopsin 2 in ganglion cells. J. Neurosci. *30*, 8745–8758.

Tomita, H., Sugano, E., Isago, H., Hiroi, T., Wang, Z., Ohta, E., and Tamai, M. (2010). Channelrhodopsin-2 gene transduced into retinal ganglion cells restores functional vision in genetically blind rats. Exp. Eye Res. *90*, 429–436.

Van Gelder, R.N. (2005). Nonvisual ocular photoreception in the mammal. Methods Enzymol. *393*, 746–755.

Vandenberghe, L.H., Bell, P., Maguire, A.M., Cearley, C.N., Xiao, R., Calcedo, R., Wang, L., Castle, M.J., Maguire, A.C., Grant, R., et al. (2011). Dosage thresholds for AAV2 and AAV8 photoreceptor gene therapy in monkey. Sci. Transl. Med. *3*, 88ra54.

Winter, J.O., Cogan, S.F., and Rizzo, J.F., 3rd. (2007). Retinal prostheses: current challenges and future outlook. J. Biomater. Sci. Polym. Ed. *18*, 1031–1055.

Yanai, D., Weiland, J.D., Mahadevappa, M., Greenberg, R.J., Fine, I., and Humayun, M.S. (2007). Visual performance using a retinal prosthesis in three subjects with retinitis pigmentosa. Am. J. Ophthalmol. *143*, 820–827.

Zhang, F., Wang, L.P., Brauner, M., Liewald, J.F., Kay, K., Watzke, N., Wood, P.G., Bamberg, E., Nagel, G., Gottschalk, A., and Deisseroth, K. (2007). Multimodal fast optical interrogation of neural circuitry. Nature *446*, 633–639.